PROCEEDINGS OF SCIENCE

Numerical Simulations of Black Hole Accretion Disks and Outflows

Ken Ohsuga

Center for Computational Sciences, University of Tsukuba,
1-1-1 Tennodai, Tsukuba, Ibaraki 305-8577 Japan

E-mail: ohsuga@ccs.tsukuba.ac.jp

Recent advances in numerical simulations have significantly revised the classical picture of accretion disks that was originally developed using one-dimensional analytic models. Radiation magnetohydrodynamic and general relativistic radiation magnetohydrodynamic simulations have become powerful tools for studying super-Eddington accretion flows around black holes. These simulations show that strong vertical radiation forces make the disk geometrically thick, while driving a multi-component outflow consisting of a fast jet near the rotation axis, a clumpy outflow at intermediate latitudes, and a failed wind along the disk surface. The observed luminosities and spectral shapes depend sensitively on the viewing angle, and by controlling accretion rate and inclination angle, many characteristic properties of ultraluminous X-ray sources can be naturally reproduced. Simulations also demonstrate that black hole spin enhances jet power and energy output through the Blandford–Znajek mechanism, and that Lense–Thirring precession occurs even in the super-Eddington regime. Further progress will require higher-resolution simulations with more accurate radiation and relativistic treatments.

87th Fujihara SeminarThe 50th Anniversary Workshop of the Disk Instability Model in Compact Binary Stars (DIM50TH2025)
22-26 September 2025
Tomakomai, Japan

 ISSN 1824-8039 . Published by SISSA Medialab.

PoS(DIM50th2025)030

1. Progress in Numerical Simulation Research

Accretion disks around black holes are widely recognized as the central engines powering a variety of luminous compact systems, including X-ray binaries and active galactic nuclei. The theoretical study of such disks has a long history, beginning with a series of one-dimensional analytic models that captured the fundamental radial structure of the flow. Among these, the standard disk, the radiatively inefficient accretion flow (RIAF), and the slim-disk solutions have played particularly influential roles [1–4]. These classical models necessarily relied on the phenomenological α-viscosity prescription to represent the disk viscosity that drives angular-momentum transport and energy dissipation - the most essential yet inherently uncertain aspects of disk dynamics.

A major conceptual breakthrough occurred when the magnetorotational instability (MRI) was identified as the physical origin of disk viscosity [5]. This discovery established magnetic fields as major components of accretion physics and led to numerical studies using magnetohydrodynamic (MHD) simulations. Three-dimensional MHD simulations were subsequently performed and demonstrated the development of MRI-driven turbulence within the disk [6–8]. Subsequent progress led to the incorporation of general relativistic effects, giving rise to GR-MHD simulations that can model gas flows in the curved spacetime surrounding spinning black holes. GR-MHD has become a powerful tool for interpreting low-luminosity black hole systems, with extensive applications to sources such as M87, where comparisons with Event Horizon Telescope (EHT) observations have become a major research frontier [9–11]

Despite their success, MHD and GR-MHD approaches are well suited only for flows with luminosities far below the Eddington limit. This is because they neglect radiative processes, including radiative heating and cooling as well as radiation-pressure forces acting on the gas. To investigate luminous disks, radiation hydrodynamics (RHD) simulations were performed by explicitly incorporating radiation transport into hydrodynamical models [12–14]. RHD methods still require an α-viscosity prescription, but such a phenomenological assumption is not needed in radiation magnetohydrodynamics (RMHD) simulations. RMHD therefore represents a first-principles framework that, in principle, can describe accretion flows regardless of the magnitude of the mass accretion rate.

Global RMHD simulations have shown that all three accretion regimes can be reproduced without fundamentally modifying the numerical framework (see Figure 1) [15, 16]. In the low-accretion-rate case, the disk becomes geometrically thick and optically thin, forming an RIAF-type flow in which magnetically driven outflows naturally emerge. At moderate accretion rates, efficient radiative cooling produces a cooler, geometrically thin disk analogous to the classical standard disk, accompanied by comparatively weak outflows. When the accretion rate greatly exceeds the Eddington limit (super-Eddington flows), radiation pressure makes the disk take on a geometrically thick structure that radiates above the Eddington luminosity; in this regime, strong radiation-pressure-driven outflows are launched from the disk surface. Ongoing developments have extended these efforts to general relativistic RMHD (GR-RMHD) simulations, enabling the study of black hole accretion flows in curved spacetime [17–19].

In this paper, we focus on super-Eddington accretion flows and the associated powerful outflows, a regime in which RMHD simulations are particularly effective, and we summarize the basic features obtained from these studies. We also present recent developments based on GR-RMHD simulations.

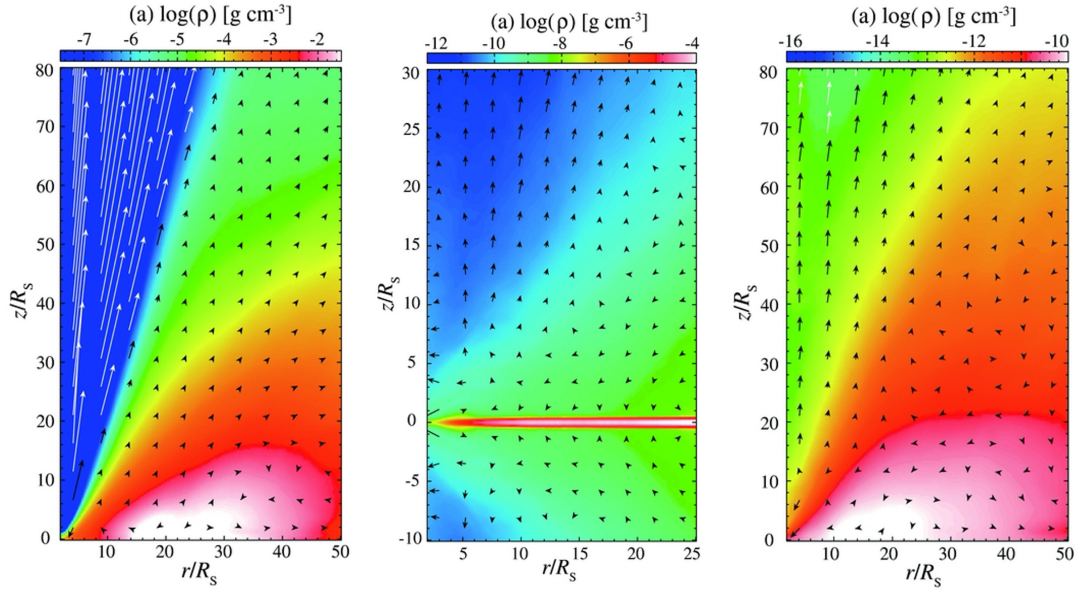

Figure 1: Three types of accretion flows obtained from RMHD simulations. Colors represent the density distribution and arrows denote the velocity field. The left panel corresponds to a super-Eddington flow, the middle panel to a standard-disk–like accretion flow, and the right panel to a RIAF-type flow. Radiation-pressure–driven outflows arise from the super-Eddington disk, while magnetically driven outflows emerge from the RIAF. Panels adapted from [16].

2. Super-Eddington Flow: Basic Properties

Super-Eddington accretion disks produce an enormous number of photons inside the disk; however, their radiative efficiency is remarkably low. The primary reason is *photon trapping*: photons generated in the dense, optically thick disk are carried inward together with the accreting matter before they can diffuse out of the flow (see Figure 2) [1, 20–22] . This situation arises when the photon diffusion timescale exceeds the radial inflow timescale, so that the trapping region typically extends to a radius of order $(\dot{M}c^2/L_{\rm Edd})\, r_{\rm g}$, where $\dot{M}$ is the mass accretion rate, $L_{\rm Edd}$ is the Eddington luminosity, c is the speed of light, and $r_{\rm g}$ is the gravitational radius, indicating that photon trapping is an essential feature of super-Eddington flows. Although the energy-conversion efficiency is drastically small, the large mass accretion rate ensures that the escaping radiation — consisting only of photons that avoid being trapped — can still exceed the Eddington luminosity.

Photons that are not trapped tend to propagate predominantly in the vertical direction rather than radially. As a result, radiation pressure does not strongly hinder gas inflow along the equatorial plane. Instead, the intense vertical radiation force puffs up the disk into a geometrically thick structure and drives radiation-pressure–dominated outflows from its surface layers. The outflow is highly wide-angled and generally becomes faster and less dense toward the disk rotation axis (see Figure 3) [23]. In the funnel region near the axis, a high-velocity flow appears with velocities of several tens of percent of the speed of light, while a surrounding layer exhibits moderately fast outflow that exceeds the escape velocity. Closer to the disk surface, however, a slower component emerges whose velocity remains below the escape velocity, forming a failed wind. Because the disk

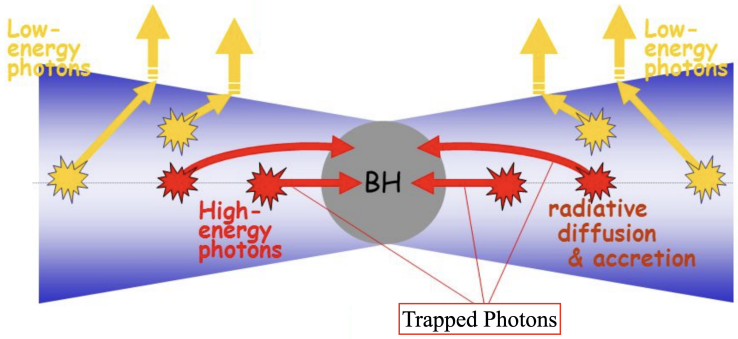

Figure 2: Schematic illustration of photon trapping. Photons generated inside the disk are advected inward together with the accreting gas and are eventually swallowed by the black hole.

is both geometrically and optically thick, photons emerging from the surface are mildly collimated toward the rotational axis as they escape. Consequently, the observed luminosity depends sensitively on the inclination angle. For example, even if the intrinsic luminosity of the disk is only a few times $L_{\rm Edd}$, a face-on observer may measure an apparent luminosity exceeding 20 $L_{\rm Edd}$.

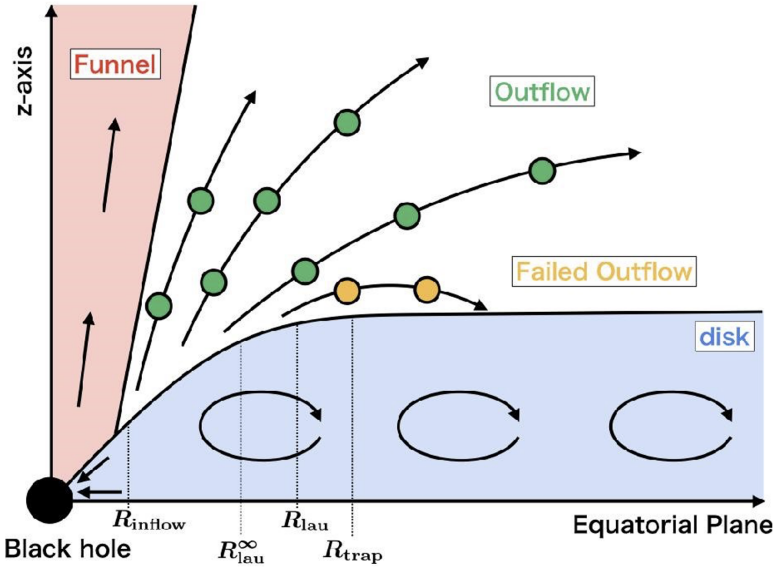

Figure 3: Schematic structure of a super-Eddington accretion flow obtained from a global RHD simulation. A geometrically thick super-Eddington disk launches a fast, low-density jet in the funnel region, a clumpy disk wind at intermediate latitudes, and a failed wind along the disk surface. Adapted from [23].

Once photons escape from the surface of a super-Eddington disk, they enter the outflowing region and undergo further processing through Compton up/down scattering. In particular, high-energy photons are efficiently produced by Compton up-scattering off the hot electrons located around the rotation axis. At the same time, photons traveling through the denser and cooler regions surrounding this hot region around the rotation axis experience significant down-scattering. As a result, the emergent spectrum depends sensitively on both the mass accretion rate and the observer's viewing angle (see Figure 4) [24, 25]. This behavior provides a possible explanation for the spectral

diversity seen in ultraluminous X-ray sources (ULXs). More recently, SED modeling based on GR-RMHD simulations has revealed a strong dependence on black hole spin: higher spin parameters tend to produce harder spectra. This trend arises because rapidly rotating black holes more readily launch powerful jets, within which Compton up-scattering becomes particularly effective [26, 27].

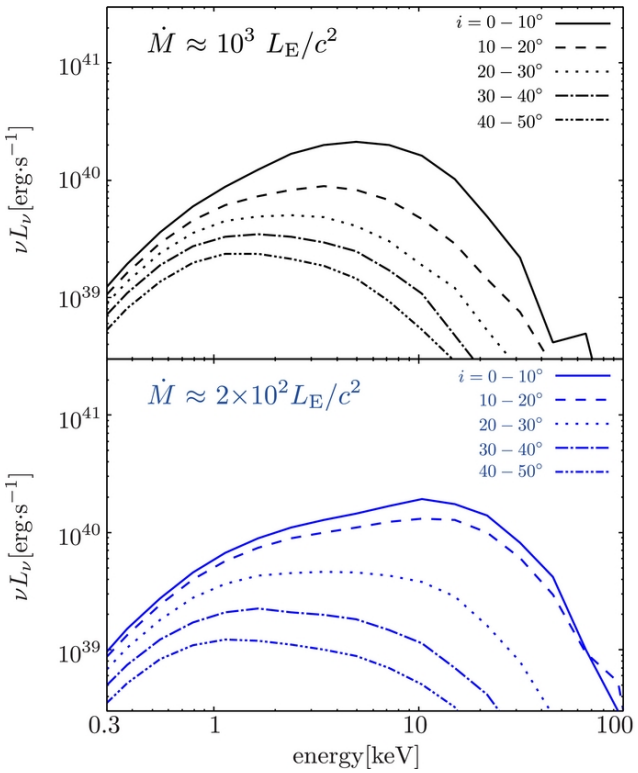

Figure 4: SEDs of a super-Eddington accretion flow obtained from radiation–transfer calculations. Photons undergo both Compton up-scattering and Compton down-scattering within the outflow. The resulting SED depends sensitively on the mass accretion rate and on the observer's viewing angle. Adapted from [24].

3. Radiation-Driven Outflows from Super-Eddington Disks

A one-dimensional model of super-Eddington disks, known as the slim-disk model, cannot describe outflows, so in this section we focus on radiation-driven outflows—one of the most important features revealed by multidimensional numerical simulations.

3.1 Radiatively-driven jets

The jet appearing in the funnel region of Fig. 3—namely, the fast and low-density component near the disk rotation axis—is driven by radiation pressure and carries tightly wound magnetic field lines, with typical terminal velocities of about 30–50% of the speed of light; they do not reach highly relativistic speeds because of *radiation drag*, a special-relativistic effect that is negligible near the disk surface but increases as the jet accelerates under the strong radiative flux, eventually balancing the radiative acceleration so that further acceleration no longer proceeds (see Figure 5) [28, 29].

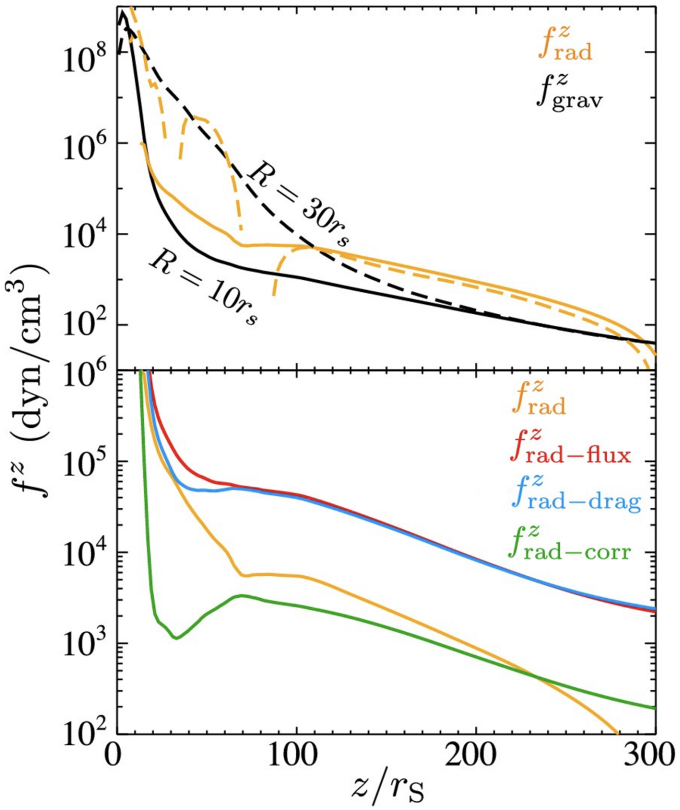

Figure 5: Vertical components of the forces obtained from an RMHD simulation. Near the disk surface ($z \sim 50\,r_{\rm S}$), the jet is accelerated mainly by the radiation flux force, whereas at higher altitudes ($z \gtrsim 100\,r_{\rm S}$), the radiation drag force becomes significant and suppresses further acceleration. Adapted from [29].

The jet speed obtained in RMHD simulations are broadly consistent with that of SS433, but they cannot account for the highly relativistic jets observed in other microquasars or in active galactic nuclei. Some GR-RMHD studies, however, have reported that highly relativistic outflows may arise when general relativistic effects are fully included, as discussed later. One might speculate that replacing baryonic matter with pair plasma would allow higher velocities by reducing inertia, but this is not correct: even if the cross section per unit mass increases, the terminal speed is still set by the balance between radiative flux force and radiative drag force, and therefore does not increase.

3.2 Clumpy disk winds

Radiation-driven outflows from super-Eddington accretion disks (outflow in Figure 3) are found to fragment into numerous gas clumps, as confirmed by RMHD simulations. The characteristic size of these clumps is typically of order $10\,r_{\rm g}$, and their outflow velocities are around $\sim 0.1c$ [30]. These values are consistent with recent XRISM observations [31]. Similar signatures of clumpy outflows have also been reported in ULXs, narrow-line Seyfert 1 galaxies, and the microquasar V404 Cygni [32–34]. Although the simulation studies discussed above primarily target ULXs and therefore assume stellar-mass black holes, recent high-resolution calculations for supermassive black holes have also shown that clumpy winds arise around super-Eddington accretion flows [35]. Further

investigations are needed to determine how the properties of these winds depend on parameters such as mass accretion rate and black hole mass.

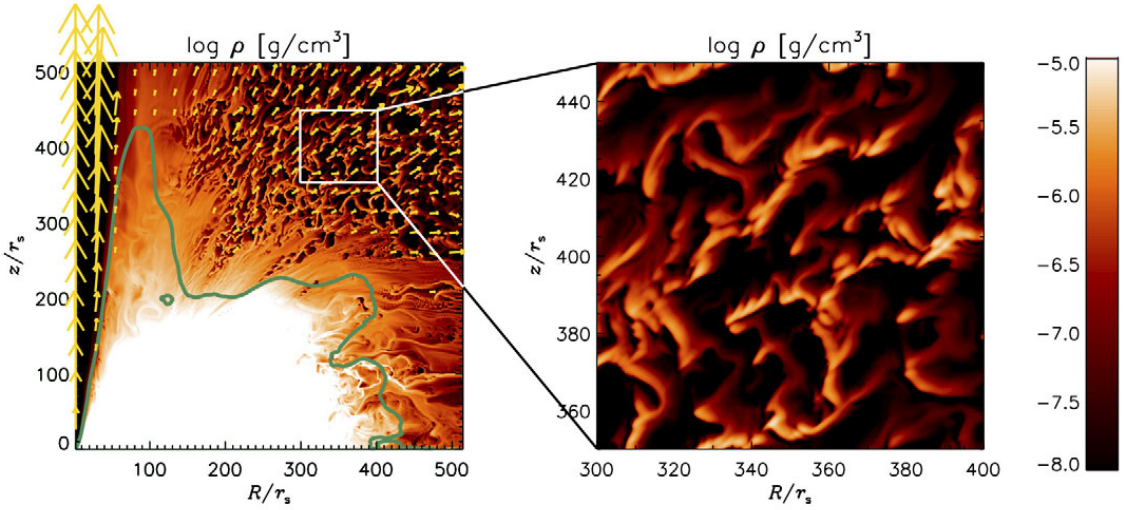

Figure 6: Clumpy disk wind obtained from an RMHD simulation. Radiation-pressure–driven outflows fragment into numerous overdense gas clumps as they propagate outward. Color represents density and arrows indicate the velocity field. Adapted from [30].

The most plausible origin of such fragmentation is the Rayleigh–Taylor (RT) instability operating in regions where radiation pressure dominates the local force balance. When the outward radiative force exceeds the inward gravitational force near the disk surface, a wind is launched while RT instability simultaneously grows, producing clumpy structures. This behavior has been confirmed by high-resolution simulations that model the disk surface layers [36]. We note that this fragmentation is not caused by MHD effects, as confirmed by these studies.

3.3 Failed disk winds

Outflows also arise near the outer edge of a super-Eddington disk, that is, around the trapping radius—often referred to as the spherization radius—which marks the boundary between the super-Eddington accretion flow and the standard disk. This outflow component streams along the disk surface, but its velocity remains below the escape velocity, and it is therefore expected to fall back onto the disk at larger radii (see the failed wind in Figure 3). Most previous numerical studies of super-Eddington accretion have focused on the inner disk region; however, recent simulations employing much larger computational domains and longer integration times have confirmed the presence of this failed wind. These studies also show that the emergence of failed winds and clumpy winds leads to substantial mass loss at radii well removed from the black hole [23, 37].

4. Impact of Black Hole Spin on Super-Eddington Accretion Flows

GR-RMHD simulations have greatly clarified how black hole spin alters both the structure of super-Eddington accretion flows and the properties of the outflows [17, 18]. GR-RMHD studies have shown that rapidly rotating black holes generate powerful jets and exhibit much larger energy

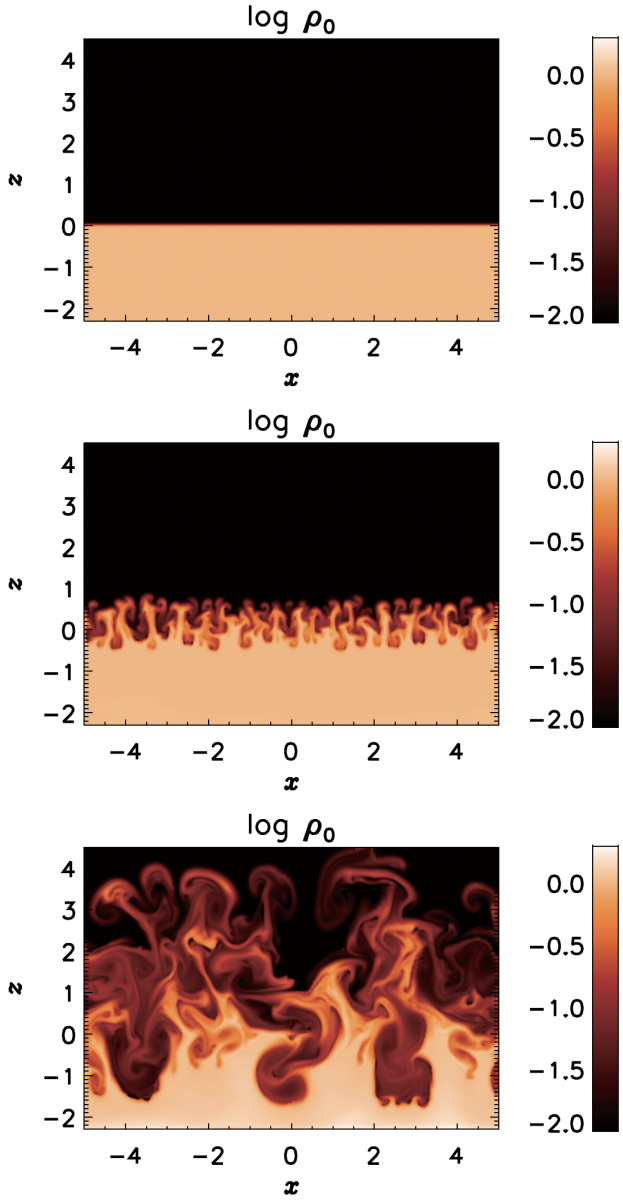

Figure 7: Growth of Rayleigh–Taylor (RT) instability in a radiation–pressure–dominated region. Upward radiation force exceeds downward gravity, so that the system is unstable. This process is considered to be a physical origin of the clumpy wind. Adapted from [36].

output, a trend that is thought to arise primarily from the Blandford–Znajek mechanism [38]. The overall energy-release efficiency—defined as the outgoing energy per unit time normalized by $\dot{M}c^2$—also increases with black hole spin, indicating that rotating black holes efficiently extract their rotational energy [41].

Further insight has been gained by examining the individual channels that contribute to the total luminosity [40]. When the black hole spin is close to zero, radiation dominates the emergent energy, while the Poynting flux carries only a minor share. As the dimensionless spin parameter grows,

however, the magnetic contribution increases rapidly. For $a_* \gtrsim 0.5$, the Poynting flux overtakes the radiative component and becomes the primary mode of energy extraction, accompanied by a significant increase in the kinetic luminosity of the jet (see Figure 8). These results demonstrate that high-spin black holes can enhance the jet power and energy output efficiency even in super-Eddington conditions.

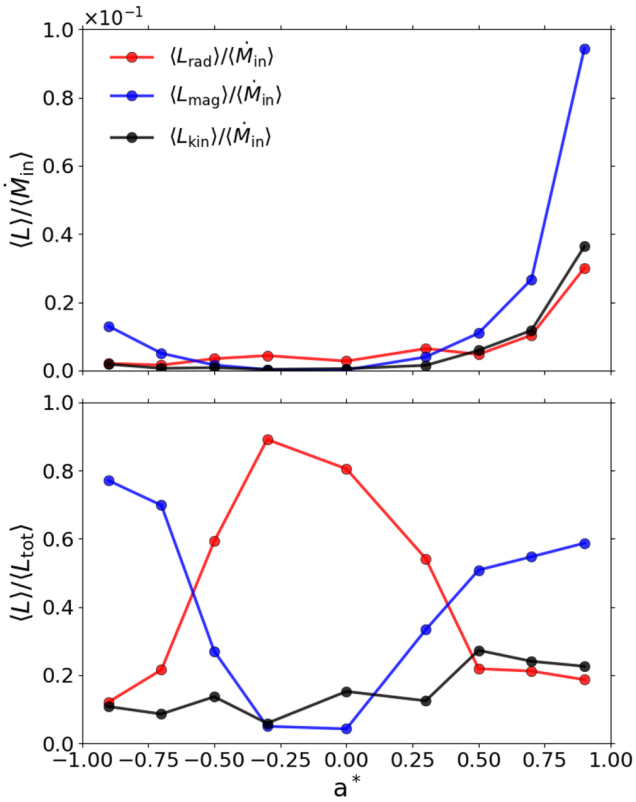

Figure 8: Black hole spin dependence of the radiative (red), magnetic (blue), and kinetic (black) energy outflow components. Top: energy outflow efficiencies. Bottom: fractional contributions of each component to the total luminosity. Adapted from [40], ApJ (CC BY 4.0).

Systems with higher black hole spin are predicted to show a larger ratio of jet kinetic luminosity to face-on X-ray luminosity, suggesting that IC 342 X-1 may host a relatively rapidly rotating black hole, whereas the central black hole in Holmberg II X-1 is more compatible with a low-spin interpretation; this ratio can also vary with changes in mass accretion rate or inclination angle [23].

The geometry of jets from spinning black holes has also been explored. Under radiatively inefficient conditions, jet shapes tend to follow a parabolic profile that becomes wider as the spin increases [41]. The relationship between jet shape and black hole spin in the super-Eddington regime has also been investigated, but the dependence remains unclear [42, 43]. Our recent GR-RMHD simulations indicate that jet shapes vary only weakly with spin, and the resulting geometries agree well with observations of a narrow-line Seyfert 1 galaxy, 1H 0323+342 (Yoshioka et al., in preparation).

Another prominent spin effect is the significant enhancement of jet velocity. Non-relativistic or pseudo-Newtonian RMHD simulations typically produce jet velocities of 0.3–0.5 c, as discussed

previously. In contrast, GR-RMHD simulations report that jets can reach Lorentz factors of order $\sim$ 10 when the black hole spin approaches unity [44]. Thus, rapid rotation can dramatically accelerate the jet.

Finally, the frame-dragging associated with a spinning black hole generates Lense–Thirring (LT) precession. Recent GR-RMHD simulations of super-Eddington flows demonstrate that the disk can become tilted and twisted, leading to outflows that precess over time (see Figure 9) [45]. Gas and radiation are emitted in directions that tend to follow the instantaneous rotation axis of the precessing disk rather than the black hole spin axis, so the outflow direction changes with the disk's precession and lags slightly behind the motion of the disk axis. This precessional behavior provides a natural explanation for the quasi-periodic oscillations observed in several ULXs [46]. The time-variable jet orientation seen in V404 Cygni may also be related to Lense–Thirring precession [47].

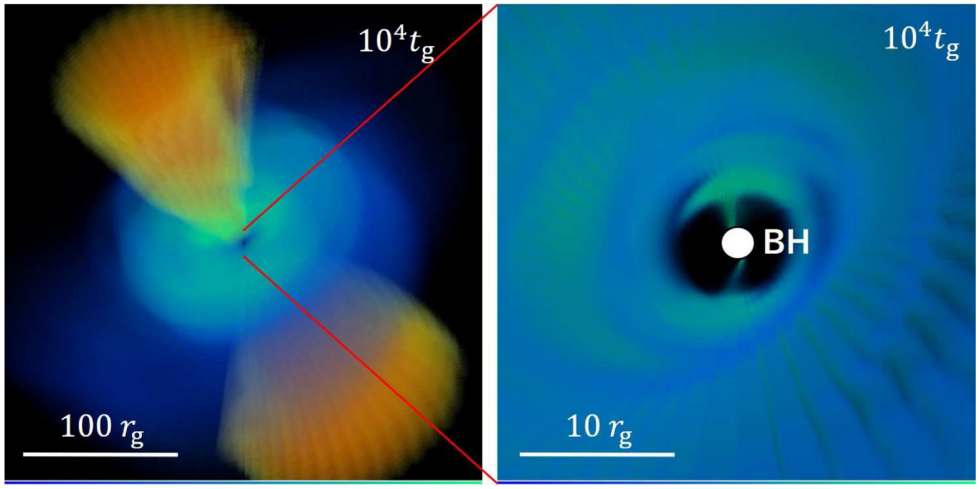

Figure 9: GR-RMHD simulation showing a precessing super-Eddington disk and jet. Both the jet and radiation are emitted preferentially along the instantaneous disk–rotation axis rather than the black hole spin axis. Adapted from [45], ApJ (CC BY 4.0).

5. Summary

Recent advances in numerical simulations have significantly deepened our understanding of accretion disks, which had long been modeled mainly through one-dimensional analytical approaches. For low-luminosity systems, MHD and GR-MHD simulations are commonly used, whereas RMHD and GR-RMHD simulations are powerful for studying high-luminosity accretion disks and their associated outflows. The main results regarding super-Eddington flows are summarized below.

- Radiation pressure drives powerful outflows from geometrically and optically thick super-Eddington disks. The outflow consists of a jet near the disk rotation axis, a surrounding clumpy outflow, and a failed wind along the disk surface.
- The apparent luminosity and SED depend sensitively on the observer's viewing angle, and by controlling the mass accretion rate and inclination, the basic properties of ULXs can be reproduced.

- Black hole spin enhances the jet power and energy output of super-Eddington systems through the Blandford–Znajek mechanism. Lense–Thirring precession caused by frame dragging can also occur in super-Eddington disks.

Numerical simulations of accretion disks and outflows remain an active and developing field, and higher-accuracy methods together with long-duration, large-domain simulations are now being developed and implemented.

References

[1] Shakura N. I., Sunyaev R. A., 1973, A&A, 24, 337

[2] Ichimaru S., 1977, ApJ, 214, 840. doi:10.1086/155314

[3] Abramowicz M. A., Czerny B., Lasota J. P., Szuszkiewicz E., 1988, ApJ, 332, 646. doi:10.1086/166683

[4] Narayan R., Yi I., 1994, ApJL, 428, L13. doi:10.1086/187381

[5] Balbus S. A., Hawley J. F., 1991, ApJ, 376, 214. doi:10.1086/170270

[6] Matsumoto R., 1999, ASSL, 240, 195. doi:10.1007/978-94-011-4780-4_62

[7] Machida M., Hayashi M. R., Matsumoto R., 2000, ApJL, 532, L67. doi:10.1086/312553

[8] Hawley J. F., Krolik J. H., 2001, ApJ, 548, 348. doi:10.1086/318678

[9] McKinney J. C., Gammie C. F., 2004, ApJ, 611, 977. doi:10.1086/422244

[10] Tchekhovskoy A., Narayan R., McKinney J. C., 2011, MNRAS, 418, L79. doi:10.1111/j.1745-3933.2011.01147.x

[11] Narayan R., Sądowski A., Penna R. F., Kulkarni A. K., 2012, MNRAS, 426, 3241. doi:10.1111/j.1365-2966.2012.22002.x

[12] Eggum G. E., Coroniti F. V., Katz J. I., 1988, ApJ, 330, 142. doi:10.1086/166462

[13] Okuda T., Fujita M., 2000, PASJ, 52, L5. doi:10.1093/pasj/52.2.L5

[14] Ohsuga K., Mori M., Nakamoto T., Mineshige S., 2005, ApJ, 628, 368. doi:10.1086/430728

[15] Ohsuga K., Mineshige S., Mori M., Kato Y., 2009, PASJ, 61, L7. doi:10.1093/pasj/61.3.L7

[16] Ohsuga K., Mineshige S., 2011, ApJ, 736, 2. doi:10.1088/0004-637X/736/1/2

[17] McKinney J. C., Tchekhovskoy A., Sadowski A., Narayan R., 2014, MNRAS, 441, 3177. doi:10.1093/mnras/stu762

[18] Sądowski A., Narayan R., McKinney J. C., Tchekhovskoy A., 2014, MNRAS, 439, 503. doi:10.1093/mnras/stt2479

[19] Takahashi H. R., Ohsuga K., Kawashima T., Sekiguchi Y., 2016, ApJ, 826, 23. doi:10.3847/0004-637X/826/1/23

[20] Begelman M. C., 1979, MNRAS, 187, 237. doi:10.1093/mnras/187.2.237

[21] Ohsuga K., Mineshige S., Mori M., Umemura M., 2002, ApJ, 574, 315. doi:10.1086/340798

[22] Ohsuga K., Mineshige S., Watarai K.-. ya ., 2003, ApJ, 596, 429. doi:10.1086/377686

[23] Kitaki T., Mineshige S., Ohsuga K., Kawashima T., 2021, PASJ, 73, 450. doi:10.1093/pasj/psab011

[24] Kawashima T., Ohsuga K., Mineshige S., Yoshida T., Heinzeller D., Matsumoto R., 2012, ApJ, 752, 18. doi:10.1088/0004-637X/752/1/18

[25] Kitaki T., Mineshige S., Ohsuga K., Kawashima T., 2017, PASJ, 69, 92. doi:10.1093/pasj/psx101

[26] Narayan R., SaÌ§dowski A., Soria R., 2017, MNRAS, 469, 2997. doi:10.1093/mnras/stx1027

[27] Pacucci F., Narayan R., 2024, ApJ, 976, 96. doi:10.3847/1538-4357/ad84f7

[28] Takeuchi S., Ohsuga K., Mineshige S., 2010, PASJ, 62, L43. doi:10.1093/pasj/62.5.L43

[29] Takahashi H. R., Ohsuga K., 2015, PASJ, 67, 60. doi:10.1093/pasj/psu145

[30] Takeuchi S., Ohsuga K., Mineshige S., 2013, PASJ, 65, 88. doi:10.1093/pasj/65.4.88

[31] Xrism Collaboration, Audard M., Awaki H., Ballhausen R., Bamba A., Behar E., Boissay-Malaquin R., et al., 2025, Natur, 641, 1132. doi:10.1038/s41586-025-08968-2

[32] Middleton M. J., Roberts T. P., Done C., Jackson F. E., 2011, MNRAS, 411, 644. doi:10.1111/j.1365-2966.2010.17712.x

[33] Jin C., Done C., Ward M., Gardner E., 2017, MNRAS, 471, 706. doi:10.1093/mnras/stx1634

[34] Motta S. E., Kajava J. J. E., Sánchez-Fernández C., Beardmore A. P., Sanna A., Page K. L., Fender R., et al., 2017, MNRAS, 471, 1797. doi:10.1093/mnras/stx1699

[35] Hu H., Inayoshi K., Haiman Z., Ho L. C., Ohsuga K., 2025, ApJL, 983, L37. doi:10.3847/2041-8213/adc680

[36] Takeuchi S., Ohsuga K., Mineshige S., 2014, PASJ, 66, 48. doi:10.1093/pasj/psu011

[37] Yoshioka S., Mineshige S., Ohsuga K., Kawashima T., Kitaki T., 2022, PASJ, 74, 1378. doi:10.1093/pasj/psac076

[38] Blandford R. D., Znajek R. L., 1977, MNRAS, 179, 433. doi:10.1093/mnras/179.3.433

[41] Narayan R., Chael A., Chatterjee K., Ricarte A., Curd B., 2022, MNRAS, 511, 3795. doi:10.1093/mnras/stac285

[40] Utsumi A., Ohsuga K., Takahashi H. R., Asahina Y., 2022, ApJ, 935, 26. doi:10.3847/1538-4357/ac7eb8

[41] Narayan R., Chael A., Chatterjee K., Ricarte A., Curd B., 2022, MNRAS, 511, 3795. doi:10.1093/mnras/stac285

[42] Curd B., Narayan R., 2023, MNRAS, 518, 3441. doi:10.1093/mnras/stac3330

[43] Curd B., Emami R., Anantua R., Palumbo D., Doeleman S., Narayan R., 2023, MNRAS, 519, 2812. doi:10.1093/mnras/stac3716

[44] Zhang L., Stone J. M., Mullen P. D., Davis S. W., Jiang Y.-F., White C. J., 2025, arXiv, arXiv:2506.02289. doi:10.48550/arXiv.2506.02289

[45] Asahina Y., Ohsuga K., 2024, ApJ, 973, 45. doi:10.3847/1538-4357/ad6cd9

[46] Atapin K., Fabrika S., Caballero-García M. D., 2019, MNRAS, 486, 2766. doi:10.1093/mnras/stz1027

[47] Miller-Jones J. C. A., Tetarenko A. J., Sivakoff G. R., Middleton M. J., Altamirano D., Anderson G. E., Belloni T. M., et al., 2019, Natur, 569, 374. doi:10.1038/s41586-019-1152-0